Journal of Renewable Materials
DOI:10.32604/jrm.2020.011462
Article

Tech Science Press

Utilization of Bayer Red Mud Derived from Bauxite for Belite-Ferroaluminate Cement Production

Yanrong Zhao[1,2,3,#], Ping Chen[1,4,*,#], Shifeng Wang[5], Yaxiong Ji[3,4], Yuanhao Wang[3,4,*], Bolin Wu[1,2] and Rongjin Liu[1]

[1]College of Material Science and Engineering, Guilin University of Technology, Guilin, 541004, China
[2]Key Laboratory of New Processing Technology for Nonferrous Metal & Materials, Ministry of Education, Guilin University of Technology, Guilin, 541004, China
[3]Guangxi Key Laboratory of New Energy and Building Energy Saving, Guilin, 541004, China
[4]Guangxi Engineering and Technology Center for Utilization of Industrial Waste Residue in Building Materials, Guilin, 541004, China
[5]Department of Physics, College of Science, Tibet University, Lhasa, 850000, China
*Corresponding Authors: Ping Chen. Email: chenping8383@188.com; Yuanhao Wang. Email: gxwangyuanhao@gmail.com.
[#]These authors contributed to the work equally and should be regarded as co-first authors
Received: 09 May 2020; Accepted: 10 June 2020

Abstract: Bayer red mud (BRM) is a kind of industrial solid waste characterized by huge volume and high alkalinity. Its disposal generates serious environmental pollution and occupies a large number of farmland. The utilization and recycling of BRM is currently a crucial issue and needs to be addressed as soon as possible. The chemical composition of BRM is similar to cement clinker. In this study, the feasibility of preparing Belite-ferroaluminate clinker (BFAC) with different BRM was explored. The physical properties, mechanics performance, radioactivity levels and trace harmful metals leaching were measured. XRD, BEI and EDS were used to characterize the mineral formation, and SEM is used to reveal the solidified mechanism of trace harmful metal. The results show that the preparation of BFAC using a certain amount of BRM was feasible. The formed phases in clinkers mainly included $C_4A_3\check{S}$, C_2S and C_4AF. The flexural strength and compressive strength of BFAC at 3 days increased whereas 28 and 90 days decreased with the increase of BRM due to the formation of higher C_4AF and lower C_2S. The formation of large amounts of $Al_2O_3{\cdot}3H_2O$ gel and $Fe_2O_3{\cdot}3H_2O$ gel in hydration products enhanced the adsorption capability to heavy metals and other ions. The trace harmful metal concentration in the leaching solution was much less than the upper limits. The radioactivity level of leaching solution was close to natural radioactive background. BRM is safe as raw material of BFAC.

Keywords: Bayer red mud; belite-ferroaluminate clinker; leaching of harmful metal; radioactivity levels; phosphogypsum

1 Introduction

At present, the world is facing unprecedented environmental challenges, and the contradiction between the shortage of resource and excessive accumulation of solid waste is increasingly prominent. The

development of the efficient, green, low-carbon and circular economy is an urgent necessity. As one of the solid waste, red mud is generated in alumina refining from bauxite [1]. Over 95% of the alumina produced all over the world is derived from bauxite extraction by the Bayer process [2]. Generally, production of 1 ton alumina will at the same time yield 1 to 1.5 tons of red mud [3]. In 2018, the total capacity of the alumina in the world and in China reached 130.43 million tons and 71.54 million tons, respectively, and the discharge of the red mud were about 150 million tons and 80 million tons, respectively. China is the largest producer of alumina. The cumulative amount of red mud in China has exceeded 350 million, which causes a terrible environmental issue [4]. To solve the problems introduced by the red mud waste, many efforts have been made. Currently, the reutilization of Bayer red mud (BRM) mainly focuses on the following aspects. Rare earths and other valuable metals can be extracted from the mud waste [5,6], but still leaving the waste with expensive processing cost. Some researchers use the red mud for wastewater treatment [5,7], however, the residue still exist. A popular recycling of the mud waste is to transform the mud into building construction materials [5]. In this case, the high alkalinity, presence of heavy metals and tiny amount of radioactive elements contained in the waste become the major concerns [1,8–10]. It is reported that the reutilization ratio of global red mud is only 15%, and that of China is less than 4% [2]. The disposal of such a large amount of red mud leads to a serious environmental threat and occupies a mass of farmland. The recycling of BRM is currently a crucial issue and needs to be addressed as soon as possible.

Calcium sulphoaluminate (CSA) cement composed of ye'elimite ($C_4A_3\check{S}$), belite (C_2S) and ferrite (C_4AF), was considered as a kind of environmentally friendly construction material, because of its less CO_2 emissions and lower energy consumption compared with Portland cement [7,11]. In addition, many other vital properties such as high early strength, shrinkage compensation, impermeability, low alkalinity and good chemical resistance have attracted researchers' attention [12–14]. However, due to the limitation of aluminum and iron material, high price, and deterioration of long-term strength, the application of CSA cement is limited [7]. At present, people pay more attention to the Belite-calcium sulfoaliminate cement (BCSA) with much lower $C_4A_3\check{S}$ and belite-ferroaluminate cement (BFAC) with higher C_4AF [7]. Low-grade bauxite or aluminum waste can be used for the preparation of clinker [15,16], which could reduce the cost and improves the long-term performance.

In BRM, the total content of Fe_2O_3, Al_2O_3, CaO and SiO_2 exceeds 70%, which makes it suitable as raw material for the preparation of cement. This work aims to use BRM, fly ash, phosphogypsum (PG), bauxite and limestone as raw materials to prepared BFAC, which possesses high early strength, excellent shrinkage compensation, outstanding impermeability, low alkalinity and good chemical resistance. Meanwhile, the production of BFAC can consume a lot of industrial solid waste, especially BRM, reducing the cost and cutting down CO_2 emissions. In this work, the feasibility of preparing BFAC with different BRM was systematically explored. The mineral composition and microstructure of clinker with varying BRM were investigated. The physical properties, mechanics performance, radioactivity levels and solidification of trace harmful metal of BFAC were measured and the solidified mechanism was studied. This work will provide a new strategy for the large-scale recycling of BRM.

2 Materials and Methods

2.1 Preparation of BFAC

The BRM was collected from Pingguo Aluminum Company (Guangxi, China). The fly ash was obtained from Laibin Power Plant (Guangxi, China). The PG was received from Wengfu (group) Co., Ltd. (Guizhou, China) and the bauxite was purchased from Shandong alumina plant (China). The limestone was supplied by Xing'an Conch Cement Co., Ltd. (Guangxi, China). The main chemical compositions of materials are presented in Tab. 1, respectively.

Table 1: Main chemical compositions of raw materials

Materials	Main chemical compositions (wt.%)									LOI* (wt.%)
	CaO	Fe_2O_3	Al_2O_3	SiO_2	SO_3	TiO_2	Na_2O	K_2O	MgO	
BRM	14.47	26.8	20.47	8.47	0.43	5.31	3.62	0.16	1.45	13.02
Fly ash	5.48	9.05	27.2	56.08	1.41	1.05	–	3.41	0.75	3.22
PG	40.17	0.13	0.96	2.36	53.0	–	–	–	–	8.86
Bauxite	1.15	1.90	64.88	12.01	1.70	3.19	–	1.18	0.61	0.56
Limestone	54.01	0.24	0.44	0.89	0.08	–	–	–	0.12	38.31

*LOI: Loss on ignition, mass loss at 1000°C.

The nitric acid (HNO_3) of GR Grade was purchased from Sinopharm Group Chemical Reagent Co., Ltd. (Shanghai, China), while the hydrofluoric acid (HF) of AR Grade and sulfuric acid (H_2SO_4) of GR Grade was purchased from Xilong Scientific Co., Ltd. (Shantou, China). The perchloric acid ($HClO_4$) of GR Grade was purchased from Damao Chemical Reagent Co., Ltd. (Tianjin, China).

The preparation of BFAC can be divided into two steps: dealkalization of BRM and preparation of cement clinker. Dealkalization was performed in a water bath. CaO was added according to the Na_2O content in BRM in order to reach the theoretical CaO-Na_2O molar ratio of 3:1. The liquid-solid ratio, agitation speed, reaction temperature and reaction time were 5:1, 320 r·min^{-1}, 80°C and 2 h, respectively. After filtration, filtrate was used to recover alkali, and then the solid sample was dried at 105°C for 6 h in an electric oven. The sodium oxide content was less than 1.0 wt.% in the dealkalized BRM (DBRM).

Three types of BFAC were prepared with 17 wt.% (A), 23 wt.% (B), 29 wt.% (C) DBRM, respectively. The content of raw materials is shown in Tab. 2.

Table 2: Ratios of raw materials and sintering temperature

Sample	Ratios of raw materials (wt.%)					Sintering temperature
	DBRM	Fly ash	PG	Bauxite	Limestone	
A	17.0	11.6	11.0	11.8	48.6	1340°C
B	23.0	8.5	11.0	12.6	44.9	1330°C
C	29.0	5.4	11.0	13.4	40.9	1320°C

In CaO-SiO_2 -Al_2O_3 -Fe_2O_3 -SO_3 system, the phases of BFAC are expected to form $C_4A_3\check{S}$ ($3CaO{\cdot}3Al_2O_3{\cdot}CaSO_4$), C_2S ($2CaO{\cdot}SiO_2$), C_4AF ($4CaO{\cdot}Al_2O_3{\cdot}Fe_2O_3$), and a small amount of associated minerals CT ($CaO{\cdot}TiO_2$) and C$\check{S}$ ($CaO{\cdot}SO_3$). Eqs. (1)–(5) were used for calculations of mineralogical phases.

$$\%C_4AF = 3.04 \times (\%Fe_2O_3) \tag{1}$$

$$\%C_2S = 2.87 \times (\%SiO_2) \tag{2}$$

$$\%C_4A_3\check{S} = 1.99 \times ((\%Al_2O_3) - 0.64 \times (\%Fe_2O_3)) \tag{3}$$

$$\%C\check{S} = 1.70 \times (\%SO_3) - 0.445 \times ((\%Al_2O_3) - 0.64 \times (\%Fe_2O_3)) \quad (4)$$

$$\%CT = 1.70 \times (\%TiO_2) \quad (5)$$

The modulus value of clinker, lime saturation factor (C), alumina oxide-sulfur trioxide ratio (P), alumina oxide—silicon dioxide (N) and alumina oxide-ferric oxide (I) were calculated by applying Eqs. (6)–(9) [2]. The results are presented in Tab. 3.

$$C = \frac{(\%CaO) - 0.7 \times (\%TiO_2)}{0.73 \times (\%Al_2O_3) - 0.64 \times (\%Fe_2O_3) + 1.40 \times (\%Fe_2O_3) + 1.87 \times (\%SiO_2)} \quad (6)$$

$$P = \frac{(\%Al_2O_3) - 0.64 \times (\%Fe_2O_3)}{(\%SO_3)} \quad (7)$$

$$N = \frac{(\%Al_2O_3) - 0.64 \times (\%Fe_2O_3)}{(\%SiO_2)} \quad (8)$$

$$I = \frac{(\%Al_2O_3)}{(\%Fe_2O_3)} \quad (9)$$

Table 3: Estimated mineralogical composition and modulus values

Sample	Estimated mineralogical composition (wt.%)						Modulus values			
	$C_4A_3\check{S}$	C_2S	C_4AF	CT	$C\check{S}$	Total	C	P	N	I
A	34.9	40.0	19.9	1.8	1.7	98.3	1.001	3.135	1.256	3.307
B	34.8	35.0	25.0	2.2	1.7	98.7	0.999	3.135	1.435	2.773
C	34.8	30.3	29.9	2.64	1.7	99.3	0.996	3,134	1.674	2.418

The raw materials were ground in ball mill to less than 80 μm in size, respectively. The raw materials were prepared by homogenizing DBRM, fly ash, PG, bauxite and limestone in certain content, and shaped into circular sample of 50 mm diameter and 5–8 mm thickness by manual tablet machine under a pressure of 3–5 MPa. Then the circular samples were sintered at certain temperature for 40 mins in high temperature box resistance furnace as shown in Tab. 2. The clinker was cooled fast by grate cooler. Finally, in order to produce cement, the clinker was mixed with 10 wt.% PG and ground to a specific surface area of 400 ± 20 m^2/kg.

2.2 Characterizations and Performance Tests

The mineralogical phases of clinker were identified using X-ray diffractometer (XRD), Scanning Electron Microscope (SEM) and energy dispersive spectrometer (EDS). The XRD tests were carried out with an "X'Pert PRO" (PANalytical B.V., Almelo, Netherlands), which was operated at 40 kV voltage and 40 mA current with a CuKa radiation source. The phases of the clinkers were identified through Gemini SEM 300 (Zeiss, Germany), equipped with an EDS detector. The harmful trace elements content of cement was detected by inductively coupled plasma optical emission spectrometry (ICP-OES), (optima 8000, perkinElmer, America). The leaching test was carried out according to Chinese National Standard GB/T 7023-2011. The cement mortar prepared in accordance with Chinese National Standard GB/T 17671-1999, and formed into cylindrical mortar samples of 50 mm diameter and 50 mm thickness (Each mortar sample contains cement of 57.0 g). The volume of leaching liquid—geometric area of the sample

ratio and leaching temperature were 10:1 cm and 25°C, respectively. The volume ratio of the nitric acid-sulfuric in the mixed acid was 2:1. Leaching of harmful elements was a slow process in practical application of cement products. To study the long-term leaching behavior of cement in a short time, the PH of leaching liquid was set to 3.2. The leaching liquid was calibrated with mixture acid once a day, and deionized water was used as a reference. The inductively coupled plasma optical emission spectrometry was used to analyze the filtered leaching solution.

The trace harmful elements composition of raw materials and cement were detected and analyzed by ICP-OES. Radioactivity levels of raw materials, clinker, leaching liquid and natural radioactive background were detected using radiation detector (IMI INSPECTOR ALERT-V2, Made in USA). The number of count rate detected by the Inspector Alert is always changing due to the random nature of radioactivity. To ensure the accuracy of test data, radiation measurement of sample was operated in Total/Timer mode to take a total count for a timed period of thirty minutes. Solid samples were kept at a certain quality of 50 grams and placed in a same metal box, whereas the leaching liquid was held in a plastic container and maintained at a fixed volume of 1 L.

3 Results and Discussion

The mineralogical phase of BRM was identified to be hematite, grandite, yugawaralite, cancrinite, gibbsite, and cristobalite, as shown in Fig. 1. The XRD patterns of A, B and C clinkers are presented in Fig. 2, and the mineral content of clinkers are estimated in Tab. 3. It is seen that the characteristic peaks of ye'elimite ($C_4A_3\check{S}$), belite (C_2S), tetracalcium alumino-ferrite (C_4AF) and perovskite (CT) are identified. In the three clinker samples, the main mineralogical phases C_4AF, $C_4A_3\check{S}$ and C_2S were well formed. A slight difference between the estimation and measurement is observed, especially in the phase of ye'elimite, the peak intensity of the ye'elimite phase and the belite phase decreases as the BRM content in the raw materials increases, whereas for the C_4AF phase holds the opposite, and more calcium alumino-ferrite phase with high iron content was found in A and B clinker, indicating that probably more Al and S participated in the formation of calcium alumino-ferrite phase with the increase of BRM content.

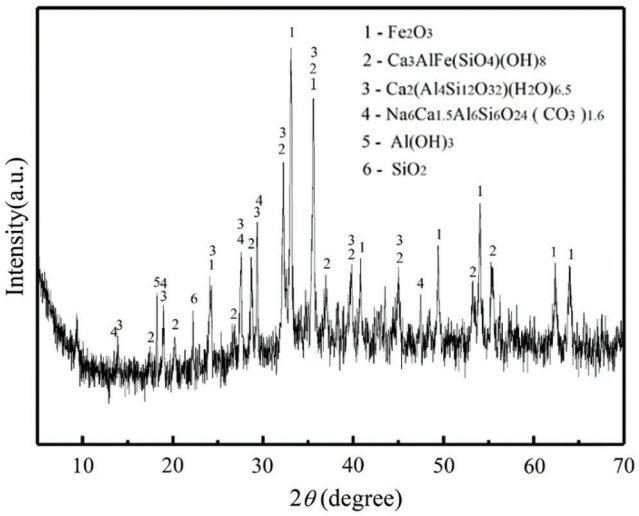

Figure 1: XRD analysis of BRM

Backscattered electron images (BEI) and energy dispersive spectrometer (EDS) analysis from the microanalysis of A, B and C clinkers are presented in Fig. 3, meanwhile, the percentage of element atoms at each point in the figure are clearly shown in Tab. 4. The BEI and EDS analysis indicate the formation

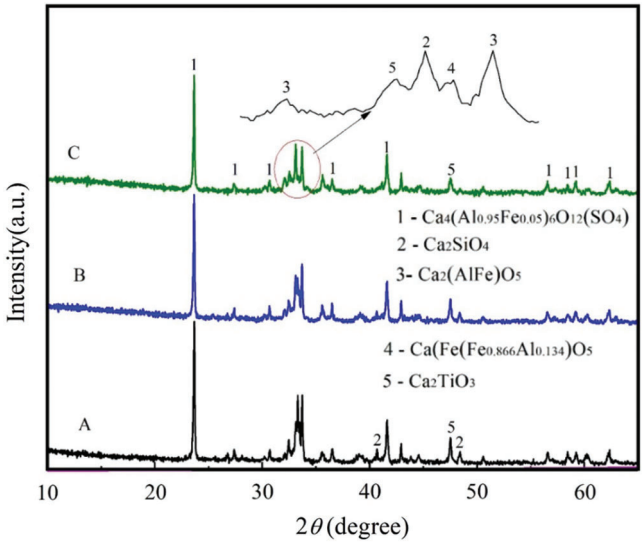

Figure 2: XRD patterns of A, B and C clinkers

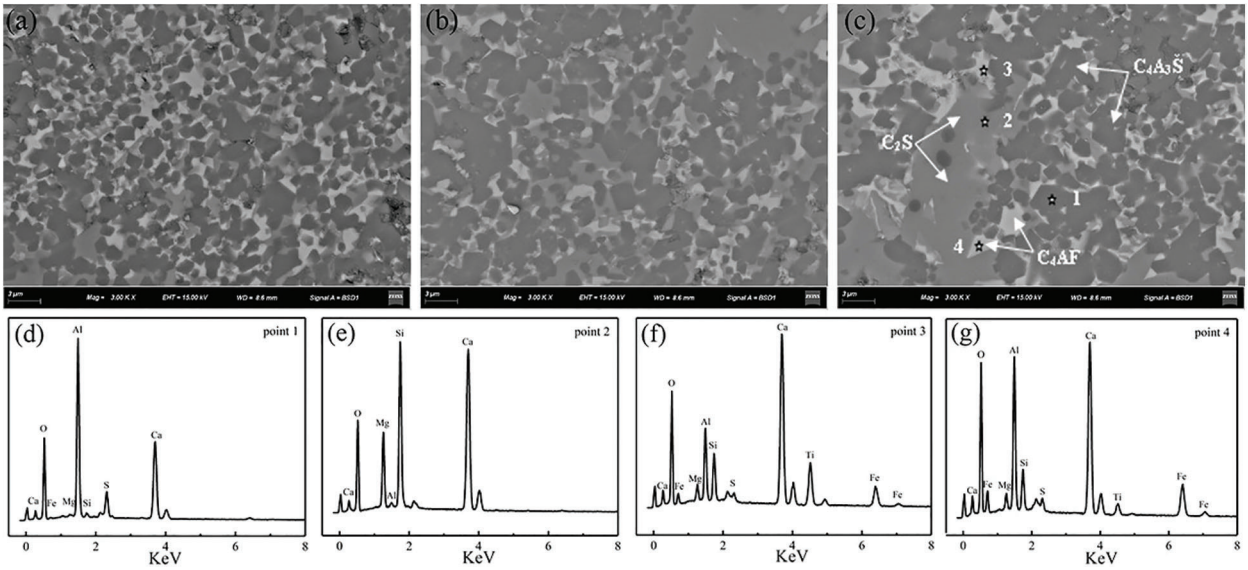

Figure 3: BEI on polished section of clinkers and EDS analysis in differing intensities of grey

Table 4: The percentage of element atoms at each point in Fig. 3

Points	Elements									
	Ca	Al	Fe	Si	S	O	Ti	Mg	Na	K
1	15.46	22.37	0.77	0.59	3.81	56.52	–	0.25	0.21	0.02
2	23.82	0.47	0.36	13.78	–	53.72	–	7.85	–	–
3	19.47	6.14	5.39	3.84	0.69	56.42	6.52	1.52	–	–
4	17.98	11.65	7.95	3.07	0.92	55.57	1.53	1.33	–	–

of the ye'elimite ($C_4A_3\check{S}$), belite (C_2S), tetracalcium alumino-ferrite (C_4AF) phases in differing intensities of grey. Oval belite grains are the largest, and the hexagonal ye'elimite crystal is the most complete, while the calcium alumino-ferrite phase is a continuous solid solution dispersed between C_2S and $C_4A_3\check{S}$.

The presence of ye'elimite, belite and tetracalcium alumino-ferrite phases are confirmed through the percentage of element atoms at each point in the figure (Tab. 4). The black areas contain high levels of O, Al, Ca and S, and low levels of Fe, Si, Mg and Na (Point 1). The atomic ratio is close to $C_4A_3\check{S}$, confirming the formation of ye'elimite, and some Mg, Na, Fe and Si are dissolved in ye'elimite instead the site of Ca, Al and S, respectively. The dark grey areas consist of O, Ca, Mg and Si in high levels, in which the atomic ratio approaches to belite (Point 2), and a small amount of Al and Fe has been found as well. A large amount of Mg is solid dissolved in the belite phase, little Al and Fe probably entering the belite lattice cause charge imbalance, which probably improves the activity of belite. The light grey areas are composed of Ca, Fe, Al, Ti, Mg and Si in high levels, little S is discovered, the mineral composition is more complicated, ratios of Ca-Fe-Al vary constantly with the change of brightness (Fig. 3 and Tab. 4), whereas tetracalcium alumino-ferrite is dominant. The above analysis further explains that the ye'elimite phase and the belite phase decrease as the BRM content in the raw materials increases.

The results of physical properties and mechanics performance of cement are presented in Tab. 5, respectively. The soundness of three samples is qualified, and the setting times of BFAC are shorter than ordinary Portland cement. As the increase of BRM in the raw materials, the setting time of cement becomes shorter, and flexural strength and compressive strength at 3 days increases whereas 28 and 90 days decreases due to the formation of higher C_4AF and lower C_2S.

Table 5: Physical properties and mechanics performance of cement

Sample	Physical properties			Flexural and compressive strength (MPa)		
	Specific surface area (m^2/kg)	Initial and Final setting time (min)	Soundness	3 days	28 days	90 days
A	412	37/80	Qualified	4.7/32.2	6.2/50.1	7.7/64.3
B	403	38/75	Qualified	4.7/33.4	5.9/48.7	7.4/61.2
C	409	35/65	Qualified	4.9/36.5	5.8/46.9	7.0/57.7

The trace harmful metal composition and radioactivity levels of raw materials and cement are shown in Tab. 6. The trace harmful metal content and radioactivity levels in BRM, bauxite and fly ash are far higher than other two materials, whereas PG and limestone are lower. The radioactivity level of raw material B is obviously declined compared to BRM due to the content decrease of BRM in raw material B, whereas increase in clinker B attributed to the concentration of trace metals and escape of gases and organic matter. The metal content of Ni, Pb, Hg and Th is obviously declined, because some of the metals are evaporated and taken away with the smoke above 1200°C.

The trace harmful metal concentration and radioactivity levels of leaching solution are given in Tab. 7. The trace harmful metal concentration of leaching solution is much less than the upper limits, and most metals are lower than the detection limit. The radioactivity levels of leaching solution are closed to the natural radioactive background of Guilin Area, China. The metal leaching rates at different periods are less than 1% in deionized water, and most metal leaching rates are below 1% even in solution with PH of 3.2, implying that the hydration products of cement play an important role in the solidification of trace harmful metal. That the solidified effect of Cr and Ba is relatively poor is over 89%. Thus, the BRM is safe as the raw material of BFAC, and cement-solidification is an effective way to treat harmful metals.

Table 6: Trace harmful metal composition and radioactivity levels

Material	Trace harmful metal content (mg/g)								RL* (CPM)
	Cr	Mn	Ba	Pb	Hg	Ni	U	Th	
BRM	1.366	0.684	0.024	0.086	0.305	0.531	2.651	0.040	130.1
Fly ash	0.086	0.419	0.491	–	–	–	0.453	–	109.0
PG	–	–	0.647	–	–	–	0.06	0.03	60.5
Bauxite	1.630	1.626	–	1.274	–	0.073	2.201	–	133.5
Limestone	1.850	1.810	–	1.040	–	0.037	–	–	56.2
Raw material B	1.410	1.121	0.118	1.04	0.061	0.037	0.902	0.012	87.4
Clinker B	0.974	0.653	0.038	0.02	0.006	–	0.883	–	94.8
Cement B	0.876	0.587	0.114	0.01	0.005	–	0.795	–	90.5

*RL: Radioactivity levels (CPM: count per minute). Natural radioactive background: 50.8 CPM.

Table 7: Trace harmful metal concentration and radioactivity levels

Leaching solution		Trace harmful metal concentration (mg/L)								RL*
		Cr	Mn	Ba	Pb	Hg	Ni	U	Th	
UL*		≤15	–	≤100	≤5	≤0.1	≤5	–	–	–
Deionized water	3 d	0.055	–	0.002	–	–	–	0.008	–	50.9
	7 d	0.108	–	0.003	–	–	–	0.027	–	51.1
	14 d	0.142	–	0.003	–	–	–	0.032	–	51.1
	30 d	0.189	–	0.002	–	–	–	0.045	–	51.4
	60 d	0.236	–	0.002	–	–	–	0.060	–	51.4
	90 d	0.241	–	0.002	–	–	–	0.081	–	51.6
	180 d	0.248	–	0.002	–	–	–	0.113	–	52.3
LR^{a}_{180} (%)		<1	<1	<1	<1	<1	<1	<1	<1	
PH = 3.2	3 d	0.056	–	0.007	–	–	–	0.013	–	51.1
	7 d	0.135	–	0.029	–	–	–	0.031	–	51.3
	14 d	0.218	–	0.074	–	–	–	0.043	–	51.2
	30 d	0.315	–	0.087	–	–	–	0.062	–	51.5
	60 d	0.401	–	0.063	–	–	–	0.089	–	52.0
	90 d	0.486	–	0.063	–	–	–	0.117	–	52.7
	180 d	0.532	–	0.066	–	–	–	0.132	–	53.0
LR^{a}_{180} (%)		<11	<1	<11	<1	<1	<1	<1	<1	

*RL: Radioactivity levels (CPM). LR^{a}_{180}: Leaching rate of harmful trace metal within a 180 days period. LR^{a} = ((Trace harmful metal content in leaching solution) * 100)/(Trace harmful metal content in cement of mortar samples), *UL: Upper limits of harmful metal in leaching solution. Natural radioactive background: 50.8 CPM.

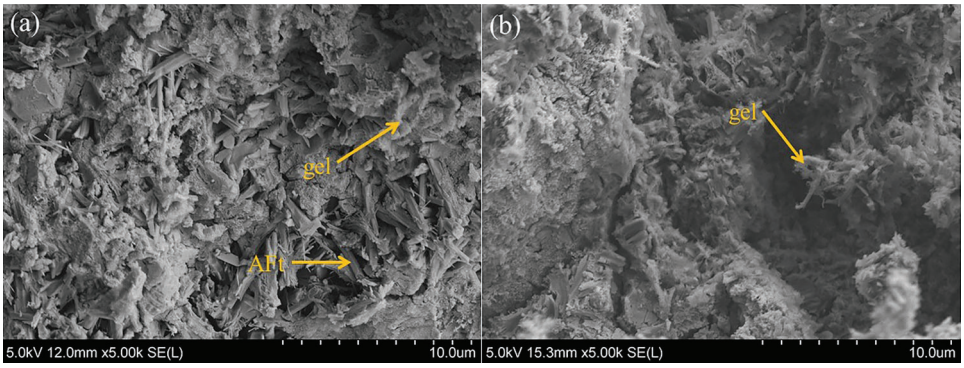

Figure 4: SEM of the hydrated production at different curing periods: (a) 3 d of B, (b) 28 d of B

SEM of sample B hydration products for 3 and 28 days are presented in Fig. 4. Needle-like, rod-like and flocculent products are very obvious for 3 days (Fig. 4a). The needle-like and rod-like products are ettringite (AFt), and flocculent products are $Al_2O_3{\cdot}3H_2O$ gel, $Fe_2O_3{\cdot}3H_2O$ gel and C-S-H gel. The reaction formula is as follows:

$$C_4A_3\check{S} + 2(CaSO_4 \cdot 2H_2O) + 34H_2O \rightarrow C_3A \cdot 3CaSO_4 \cdot 32H_2O + 2(Al_2O_3 \cdot 3H_2O)\ (gel) \tag{10}$$

$$C_4AF + 3(CaSO_4 \cdot 2H_2O) + 30H_2O \rightarrow C_3(xA \cdot (1-x) \cdot F) \cdot 3CaSO_4 \cdot 32H_2O + Ca(OH)_2 + (1-x)(Al_2O_3 \cdot 3H_2O)(gel) + x(Fe_2O_3 \cdot 3H_2O)\ (gel) \tag{11}$$

$$C_2S + 2H_2O \rightarrow C\text{-}S\text{-}H\ (II) \tag{12}$$

The flocculent gel increases for 28 days, the microstructure of ettringite changes from rod-like for 3 days to fine needle-like for 28 days (Fig. 4b). Flocculent hydration products have large surface area, high pore volume, and strong adsorption capacity [4]. The hydration products of C_4AF contain a large number of $Al_2O_3{\cdot}3H_2O$ gel and $Fe_2O_3{\cdot}3H_2O$ gel, and increases the density of cement by filling. Thus, we speculate that trace harmful metals are easily absorbed and solidified in cement products, and only a small amount of loosely consolidated metal enters the solution through connected pores. In addition, C2S in BFAC contains a certain amount of Fe and Al instead of Si, this charge imbalance still exists in the hydration products, and it is easy to absorb some other ions.The above analysis may explain this reason of cement-solidification.

4 Conclusion

In this study, a kind of BFAC clinkers were prepared using BRM, and the mineral composition, microstructure, physical properties, mechanics performance, radioactivity levels and trace harmful metals leaching were measured, and the solidified mechanism was analyzed. It can be concluded as follows:

i) It is feasible to prepare BFAC clinkers using a certain amount limestone, fly ash, bauxite, PG together with 17 wt.% (A), 23 wt.% (B) and 29 wt.% (C) DBRM at sintering temperature of 1340°C, 1330°C and 1320°C, sintering time of 40 mins, respectively.

ii) The C_4AF phase content increases as BRM content in the raw materials increase whereas $C_4A_3\check{S}$ phase and C_2S phase content decreases compared to the calculated content, because calcium alumino-ferrite phase is a continuous solid solution dispersed between C_2S and $C_4A_3\check{S}$, and a certain amount of S and Si which format $C_4A_3\check{S}$ and C_2S is dissolved in the calcium alumino-ferrite phase.

iii) The flexural strength and compressive strength at 3 days increases with the increase of DBRM in the raw materials, whereas 28 and 90 days decreases due to the formation of higher C_4AF and lower C_2S.

iv) BRM is safe as the raw material of BFAC production. Flocculent hydration products with large surface area and high pore volume able to absorb most trace harmful metal, the formation of large amounts of $Al_2O_3 \cdot 3H_2O$ gel and $Fe_2O_3 \cdot 3H_2O$ gel increases the density of cement, the charge imbalance caused by unequal substitution in C2S also increases the adsorption capacity of the products, and the trace harmful metal concentration of leaching solution is much less than the upper limits. The leaching rates are below 11% even in solution with PH of 3.2.

Acknowledgement: Special thanks to researcher Wenfeng Zhu, for his kind help in experimentation, and the BEI, EDS and SEM tests, respectively.

Funding Statement: This study was financially supported by the Guangxi Science and Technology Plan project of China (Grant No. 2018GXNSFBA138053, No. 2018AA23004); Guangxi Young and Middle-aged Teachers Basic Ability Promotion Project (Grant No. 2017KY0250); Key Laboratory of New Processing Technology for Nonferrous Metal & Materials, Ministry of Education (Grant No. 19AA-13); and Guangxi Key Laboratory of New Energy and Building Energy Saving (Grant No. 19-J-21-24).

Conflicts of Interest: The authors declare that they have no conflicts of interest to report regarding the present study.

References

1. Liu, W., Chen, X., Li, W., Yu, Y., Yan, K. (2014). Environmental assessment, management and utilization of red mud in China. *Journal of Cleaner Production, 84,* 606–610. DOI 10.1016/j.jclepro.2014.06.080.
2. Mukiza, E., Zhang, L., Liu, X., Zhang, N. (2019). Utilization of red mud in road base and subgrade materials: a review. *Resources, Conservation and Recycling, 141,* 187–199. DOI 10.1016/j.resconrec.2018.10.031.
3. Liu, R. X., Poon, C. S. (2016). Utilization of red mud derived from bauxite in self-compacting concrete. *Journal of Cleaner Production, 112,* 384–391. DOI 10.1016/j.jclepro.2015.09.049.
4. Chen, X., Guo, Y., Ding, S., Zhang, H., Xia, F. et al. (2019). Utilization of red mud in geopolymer-based pervious concrete with function of adsorption of heavy metal ions. *Journal of Cleaner Production, 207,* 789–800. DOI 10.1016/j.jclepro.2018.09.263.
5. Khairul, M. A., Zanganeh, J., Moghtaderi, B. (2019). The composition, recycling and utilisation of Bayer red mud. *Resources, Conservation and Recycling, 141,* 483–498. DOI 10.1016/j.resconrec.2018.11.006.
6. Liu, W., Yang, J., Xiao, B. (2009). Application of Bayer red mud for iron recovery and building material production from alumosilicate residues. *Journal of Hazardous Materials, 161(1),* 474–478. DOI 10.1016/j.jhazmat.2008.03.122.
7. Huang, Y., Qian, J., Kang, X., Yu, J., Fan, Y. et al. (2019). Belite-calcium sulfoaluminate cement prepared with phosphogypsum: influence of P_2O_5 and F on the clinker formation and cement performances. *Construction and Building Materials, 203,* 432–442. DOI 10.1016/j.conbuildmat.2019.01.112.
8. Zhang, R., Zheng, S., Ma, S., Zhang, Y. (2011). Recovery of alumina and alkali in Bayer red mud by the formation of andradite-grossular hydrogarnet in hydrothermal process. *Journal of Hazardous Materials, 189(3),* 827–835. DOI 10.1016/j.jhazmat.2011.03.004.
9. Kumar, A., Kumar, S. (2013). Development of paving blocks from synergistic use of red mud and fly ash using geopolymerization. *Construction and Building Materials, 38,* 865–871. DOI 10.1016/j.conbuildmat.2012.09.013.
10. Liu, Z., Li, H. (2015). Metallurgical process for valuable elements recovery from red mud—a review. *Hydrometallurgy, 155,* 29–43. DOI 10.1016/j.hydromet.2015.03.018.
11. Ma, J., Yu, Z., Ni, C., Shi, H., Shen, X. (2019). Effects of limestone powder on the hydration and microstructure development of calcium sulphoaluminate cement under long-term curing. *Construction and Building Materials, 199,* 688–695. DOI 10.1016/j.conbuildmat.2018.12.054.
12. Li, G., Zhang, J., Song, Z., Shi, C., Zhang, A. (2018). Improvement of workability and early strength of calcium sulphoaluminate cement at various temperature by chemical admixtures. *Construction and Building Materials, 160,* 427–439. DOI 10.1016/j.conbuildmat.2017.11.076.

13. Yu, J., Qian, J., Tang, J., Ji, Z., Fan, Y. (2019). Effect of ettringite seed crystals on the properties of calcium sulphoaluminate cement. *Construction and Building Materials, 207,* 249–257. DOI 10.1016/j.conbuildmat.2019.02.130.
14. Wang, Y., Zhang, T. A., Lyu, G., Guo, F., Zhang, W. et al. (2018). Recovery of alkali and alumina from bauxite residue (red mud) and complete reuse of the treated residue. *Journal of Cleaner Production, 188,* 456–465. DOI 10.1016/j.jclepro.2018.04.009.
15. Yang, L., Yan, Y., Hu, Z., Xie, X. (2013). Utilization of phosphate fertilizer industry waste for belite-ferroaluminate cement production. *Construction and Building Materials, 38,* 8–13. DOI 10.1016/j.conbuildmat.2012.08.049.
16. Iacobescu, R. I., Pontikes, Y., Koumpouri, D., Angelopoulos, G. N. (2013). Synthesis, characterization and properties of calcium ferroaluminate belite cements produced with electric arc furnace steel slag as raw material. *Cement and Concrete Composites, 44,* 1–8. DOI 10.1016/j.cemconcomp.2013.08.002.